Implementation of a direct-imaging and FX correlator for the BEST-2 array

G. Foster,[1,2]★ J. Hickish,[1] A. Magro,[3] D. Price[1,4] and K. Zarb Adami[1,2]

[1]*Sub-Department of Astrophysics, Department of Physics, University of Oxford, Denys Wilkinson Building, Keble Road, Oxford OX1 3RH, UK*
[2]*Department of Physics and Electronics, Rhodes University, PO Box 94, Grahamstown 6140, South Africa*
[3]*Department of Physics, University of Malta, Msida MSD 2080, Malta*
[4]*Harvard–Smithsonian Center for Astrophysics, 60 Garden Street, Cambridge, MA 02138, USA*

ABSTRACT

A new digital backend has been developed for the Basic Element for SKA Training II (BEST-2) array at Radiotelescopi di Medicina, INAF-IRA, Italy, which allows concurrent operation of an FX correlator, and a direct-imaging correlator and beamformer. This backend serves as a platform for testing some of the spatial Fourier transform concepts which have been proposed for use in computing correlations on regularly gridded arrays. While spatial Fourier transform-based beamformers have been implemented previously, this is, to our knowledge, the first time a direct-imaging correlator has been deployed on a radio astronomy array. Concurrent observations with the FX and direct-imaging correlator allow for direct comparison between the two architectures. Additionally, we show the potential of the direct-imaging correlator for time-domain astronomy, by passing a subset of beams though a pulsar and transient detection pipeline. These results provide a timely verification for spatial Fourier transform-based instruments that are currently in commissioning. These instruments aim to detect highly redshifted hydrogen from the epoch of reionization and/or to perform wide-field surveys for time-domain studies of the radio sky. We experimentally show the direct-imaging correlator architecture to be a viable solution for correlation and beamforming.

Key words: instrumentation: interferometers – instrumentation: miscellaneous – techniques: interferometric – radio continuum: general.

1 INTRODUCTION

We present a new digital backend designed for the Basic Element for SKA Training II (BEST-2) array at the Radiotelescopi di Medicina, INAF-IRA, Italy. This backend is implemented on Field Programmable Gate Array (FPGA)-based hardware from the Collaboration for Astronomy Signal Processing and Electronics Research (CASPER[1]; Parsons et al. 2006). It consists of an FX correlator and a spatial fast Fourier transform (FFT) processor which can be used as a direct-imaging correlator or as a beamformer, supplying high time resolution data to a pulsar and transient detection pipeline.

Within radio astronomy, sensitivity, field of view and resolution requirements drive an upward trend in the size of correlators. In recent years, many new arrays (for example: PAPER,[2] MWA,[3]

LEDA,[4] LOFAR[5]) have been deployed with the goal of detecting highly redshifted hydrogen in the early Universe. These low-frequency arrays are made up of $O(100)$ cross-correlated antenna elements (or beamformed 'stations'); their sensitivity is limited by total collecting area of these elements. Increasing the number of antennas per array without a reduction in field of view requires a larger correlator, the cost of which scales as $O(N^2)$, where N is the number of stations/elements. Next-generation telescopes, such as the HERA-II array,[6] and the Square Kilometre Array (SKA)[7] will require order of magnitude larger N-correlators, and correspondingly the computational requirements of their correlators are significantly higher.

Where arrays have stations which are regularly distributed, direct-imaging correlators can take advantage of array redundancy to reduce correlation cost scaling to $O(N \log N)$. This is achieved by

---

★E-mail: griffin.foster@gmail.com
[1] https://casper.berkeley.edu
[2] http://eor.berkeley.edu
[3] http://www.mwatelescope.org

[4] http://www.21cmcosmology.org
[5] http://www.lofar.org
[6] http://www.reionization.org
[7] http://www.skatelescope.org

directly producing images of the sky using multi-dimensional spatial FFTs. By zero-padding the spatial FFT inputs, a correlation matrix of all unique uv samples can be recovered after time integration by applying an inverse Fourier transform to this image. Though the idea of direct image formation by spatial FFT is not new in astronomy (see, for example, Otobe et al. 1994), retention of all uv data by prior zero-padding is a relatively recent proposal (Tegmark & Zaldarriaga 2009, 2010). The Tegmark & Zaldarriaga (2010) method has been extended, at an increase in computational cost, to accommodate non-regular arrays in Morales (2011) and Bunton (2011). To our knowledge, this BEST-2 backend represents the first deployment of a direct-imaging telescope which implements the design proposed by Tegmark & Zaldarriaga (2009).

For epoch of reionization (EoR) power spectrum studies, there are advantages in carefully designed maximally redundant arrays, as is discussed in Parsons et al. (2012). PAPER, CHIME,[8] and MiTEoR[9] are all regularly gridded arrays, and regularly gridded layouts are being considered for the HERA-II array. Nevertheless, it must first be verified that direct-imaging correlators can deliver calibrated science-quality data products.

A challenge of the direct-imaging correlator architecture is that calibration solutions for individual antennas must be applied during the observation; they cannot be applied post-correlation as the spatial FFT effectively averages all redundant baselines together. By developing a direct-imaging correlator, we have explored the calibration challenge in a practical way. We show that with a stable system the direct-imaging correlator, once calibrated, can produce viable images, visibilities and beams to be used for scientific observation.

The rest of this section provides a review of how the spatial Fourier transform can be used as the basis for the direct-imaging correlator. In addition, we include an overview of the BEST-2 array, which serves as a suitable direct-imaging front end. Section 2 is a detailed overview of the FPGA-based system on which the BEST-2 backend is implemented. In Section 3, we present the results of initial observations with the backend, including images from both the direct-imaging and FX correlator systems, and a preliminary pulsar observation.

1.1 Correlation using a spatial Fourier transform

An FX correlator computes the Fourier transform of time-domain antenna signals (the *F* operation) and then forms uv samples by per-channel, per-sample cross-multiplication of all antenna signal pairs (the *X* operation). For an antenna array with N elements, there are $O(N^2)$ such combinations of antenna pairs, which give rise to an $O(N^2)$ computational cost of FX correlators.

The formation of uv samples by cross-multiplication is equivalent to a spatial autocorrelation of channelized antenna signals. This can be implemented by performing a per-channel, per-sample spatial Fourier transform on the channelized signals from the antennas in an array, then taking the element-wise power of the result, and finally inverse Fourier transforming the result (after averaging over time) to recover the cross-power spectrum. The direct-imaging correlator is a correlator that performs precisely these steps, and is so named because, prior to the final inverse Fourier transform, the intermediate data product is an image of the sky. In this sense, a direct-imaging correlator is not really a correlator at all, but rather

a beamformer capable of forming enough beams simultaneously to obtain a complete image of the sky.

In general, the largest number of independent uv measurements which can be made by an array of N elements is of order N^2. The direct-imaging correlator provides an opportunity to perform these measurements by forming an equivalent number of beams on the sky rather than computing correlations directly.

When N receiving elements in an antenna array are placed on a regularly spaced grid, only $O(N)$ independent uv measurements are obtained, since many of the two-element interferometers in the array are redundant. It is thus possible to encapsulate all of these measurements in $O(N)$ beams. These could be formed by simple discrete Fourier transform and power detection, which has a computational cost of $O(N)$ operations per beam. However, a well-known method for producing a complete set of orthogonal beams on the sky from regularly spaced antennas is by spatial FFT beamforming (Williams 1968). Such a beamforming implementation is able to generate N beams on the sky, at a computational cost of $O(N \log N)$. For large-N arrays, this can be a significant computational saving compared to imaging by FX correlation which requires $O(N^2)$ operations to compute all $O(N^2)$ pairwise antenna correlations.

Essentially the only difference between the imaging methods outlined by Tegmark & Zaldarriaga (2009) and the FFT beamforming of Williams (1968) is that the former requires zero-padding to be applied to the matrix of antenna signals before the spatial FFT is performed. In a physical sense, this ensures that enough (real-valued) beam powers are measured to encode all the (complex-valued) uv-plane information which would be measured by a correlator. The zero-padding required results in the generation of $2^m N$ beams on the sky, where m is the number of dimensions in the antenna array. In the BEST-2 case, $m = 2$.

It is worth reiterating what a uv measurement represents in terms of the direct-imaging correlator. Instead of making individual measurements of redundant two-element interferometers in an array (as in an FX correlator), the direct-imaging correlator computes an 'effective' visibility which is the average of the visibilities in a redundant set of interferometers. But, for the average visibility to effectively represent the sky uv mode being measured, each redundant-baseline measurement must be identical. Thus, calibration to the complex gains must be applied before the direct-imaging operation. Further calibration can be applied after imaging, but comes with the penalty of reduced signal-to-noise. We will consider what implications this has on observations in a future work comparing the FX and direct-imaging correlators.

1.2 BEST-2 array

The BEST-2 array consists of eight east–west oriented cylindrical concentrators, each with 64 dipole receivers critically sampling a focal line at 408 MHz. Signals from these 64 dipoles are analogue beamformed in groups of 16, resulting in 4 receiver channels per cylinder, and a total of 32 effective receiving elements laid out on a 4×8 grid, depicted in Fig. 1(a). The cylinders, which lie on an east–west axis, can be rotated to point at a constant declination within the array pointing limits. A synopsis of the BEST-2 array specifications is presented in Table 1. BEST-2 was developed as a reliable, low-cost analogue front end to be used in SKA development, with a core design requirement of simplicity in interfacing with different digital backends (Montebugnoli et al. 2009b). Extensive documentation of the development of the BEST-2 analogue chain can be found in several earlier publications (Perini 2009; Perini et al. 2009).

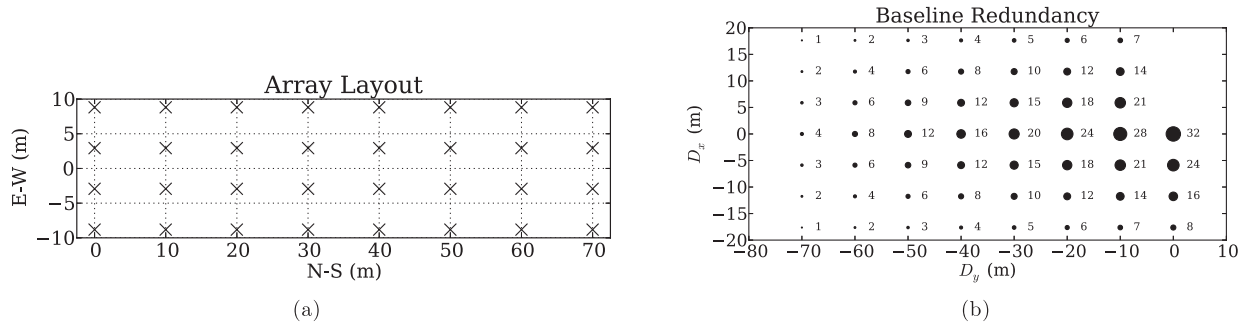[8] http://chime.phas.ubc.ca
[9] Zheng et al. (2013).

Figure 1. BEST-2 array configuration. Panel (a) shows the array layout of the eight cylindrical antennas each with four effective receivers of 16 beamformed dipoles. The array is on a *4-by-8* grid. Panel (b) shows the array baseline redundancy; circle radius shows the relative baseline redundancy and values indicate number of redundant baselines for a given length. There are 53 unique baselines. This is also the effective uv coverage for a source at the local meridian.

Table 1. The top level specifications of the BEST-2 array, a subset of the Northern Cross, located near Medicina, Italy. The array is in a regularly gridded 4×8 layout.

BEST-2 array specifications	
Total number of receivers	32
Total collecting area	$1411.2 \, \text{m}^2$
$A_{\text{eff}}/T_{\text{sys}}$	$11.65 \, \text{m}^2/\text{K}$
Longest baseline (E-W)	17.04 m
Longest baseline (N-S)	70.00 m
Central frequency	408 MHz
Analogue bandwidth	16 MHz
Primary beam area	58.6 deg^2
North–south	6°86
East–west	8°77
Zenith-pointing PSF area	$\frac{1}{3}$ deg^2
North–south	16 arcmin
East–west	75 arcmin

Table 2. Specification of the digital instrument made of the F-Engine, S-Engine and X-Engine boards which implement the direct-imaging and FX correlator architectures.

Digital hardware specifications	
Digital bandwidth	20 MHz
ADC sampling	12-bit
PFB-FIR	4-tap Hann window
PFB-FFT	2048 radix-2
Freq. channel width	19.53 kHz
Quantization	4-bit complex
X-Engine	
Autocorrelations	32
Cross-correlations	496
min τ_{int}	6.55 ms
S-Engine	
2D FFT	8×16
Selectable beams	128
Unique baselines	53
min τ_{int}	1 s

The gridded layout of the array is a key requirement of the direct-imaging correlator architecture. This grid structure leads to a highly redundant array, Fig. 1(b), where there are $\sim 2N$ unique baselines. A direct-imaging correlator architecture produces all the unique baselines where any 'effective baseline' is the average of all the redundant baselines for that baseline length and projection. The gridded layout also produces regular uv coverage, Fig. 1(b), of a field which leads to strong sidelobe in the point spread function (PSF) which can be seen in the images.

2 FPGA INSTRUMENTATION

The new FPGA-based instrumentation we have developed has replaced the previous-generation FX correlator system which used CASPER iBOB and BEE2 boards (Montebugnoli et al. 2009a). The new instruments have been implemented on FPGA-based Reconfigurable Open Architecture Computing Hardware (ROACH) boards also developed by CASPER. The ROACH platform is based on a XILINX Virtex 5 SX95T FPGA with interfaces to dynamic random-access memory and quad data rate (QDR) static random-access memory, high-speed CX-4 connectors and a generic Z-DOK interface for connecting analogue-to-digital converters (ADCs) and various other daughter boards. Digital signal processing (DSP) components of the firmware were developed using MATLAB Simulink, the CASPER DSP libraries and custom Hardware Description

Language code. Firmware models, bitstreams and control software are available from our project repository.[10]

The instrument is made up of three interconnected ROACH boards. These will be referred to as the F-Engine, S-Engine and X-Engine for their respective functions. Signal digitization and frequency channelization are performed on the F-Engine. Duplicate streams are sent to the X-Engine for cross-correlation, and to the S-Engine where a spatial Fourier transform is performed. Table 2 lists the digital specifications of the implemented FPGA hardware. Block diagrams of the firmware for each board are included in a supplemental online appendix.

2.1 F-Engine

Both correlators use the same digitization and channelization front end. The F-Engine processing node is responsible for digitization, channelization and transmission of quantized antenna signals to downstream processing boards. Duplicate streams are sent from the F-Engine to the S-Engine and X-Engine so that the correlators may be used concurrently. This allows for a streamlined process for calibrating the direct-imaging correlator data and simultaneous

[10] https://github.com/griffinfoster/medicina

observation with both correlators, and reduces the amount of hardware.

2.1.1 Digitization

In the analogue chain, the radio frequency signal, centred at 408 MHz, is mixed down with an 378 MHz local oscillator to an intermediate frequency of 30 MHz. Prior to digitization, the last amplifier stage of the analogue chain has per-signal channel adjustable gain useful for setting levels for optimum ADC quantization. Signal digitization is performed using the CASPER 64ADCx64-12[11] analogue-to-digital converter (ADC) board which makes use of the Texas Instruments ADS5272 8-channel, 12-bit ADC chip. In the case of the 64ADCx64-12, eight ADS5272 ADC chips are used to digitize 64 analogue inputs at up to 50 Msps. The 64ADCx64-12 board interfaces with the ROACH over 64 low-voltage differential signal pairs via Z-DOK. In our design, 32 signal streams are digitized at 40 Msps for 20 MHz of digital bandwidth which covers the 16 MHz analogue band.

2.1.2 Channelization

In order to facilitate the correlation and imaging processing described in Section 1.1, antenna signals must be split into multiple frequency channels. These channels should have narrow enough bandwidth that they can be treated as monochromatic. This leads to the requirement that the relative arrival time of radiation at different antennas in the array should be much shorter than the inverse bandwidth of each channel. In the most stringent case of radiation arriving from the horizon, we require

$$\frac{1}{B} = \alpha \frac{D}{c}, \qquad \alpha \gg 1, \qquad (1)$$

where B is the bandwidth of a frequency channel, D is the largest dimension of the array and c is the speed of light. For the BEST-2 array, $D = 70$ m which with $k = 10$ sets a minimum channel bandwidth of approximately 400 kHz.

The strong radio frequency interference environment at the observatory sets a more restrictive demand for narrow channel widths and high out-of-band rejection that is achieved by use of a polyphase filterbank (PFB). Our digitized band is channelized using a critically sampled 4-tap Hann filter, 2048-point PFB (using 18-bit coefficients) to produce 1024 complex samples per real antenna stream covering the range 398–418 MHz. Individual channel resolution is 19.53 kHz. The ROACH-I board is clocked at 160 MHz, four times the ADC sample rate, such that four signals are time-division multiplexed on to a single signal path.

2.1.3 Equalization and quantization

After channelization the samples are requantized to 4-bit complex values. This limits the F-Engine output data rate to 5.12 Gbps. See section 8.3 of Thompson, Moran & Swenson (2004) for details on the effect of quantization noise in a 4-bit system.

The characteristics of a telescope analogue front end mean that a compensation of the instrumental bandpass must be applied to data to ensure optimal quantization of all sub-bands. In the BEST-2 backend, this equalization is achieved by pre-multiplying the 18-bit data

streams by a set of 18-bit coefficients, with 512 independent coefficients available to represent the bandpass of each analogue channel. During observations, an automated script samples the pre-quantized signals and statistically determines the correct equalization coefficients to achieve optimal 4-bit quantization. This script can be run at a user selected cadence during observations.

The per-channel equalizers are also used to apply pre-derived amplitude and phase corrections to the signals before the 2D FFT. These values can by dynamically set during observations to account for changes in the system calibration. Duplicate streams, though with different ordering, are sent over X Attachment Unit Interface at a rate of 5.12 Gbps to the X-Engine and S-Engine nodes.

2.2 X-Engine

An FX correlator architecture is a standard design for large-bandwidth, many antenna arrays. An overview of the architecture is presented in Romney (1999). The core component to the *X* stage of the FX correlator is the complex multiply and accumulate of all pairs of independent signals for each frequency channel. A pipelined X-Engine, based on the general CASPER block (Urry et al. 2007), is used for optimal multiplier efficiency.

The correlation is performed on a per-channel basis; thus, the channelized band can be split up into portions and processed in parallel across multiple X-Engines. This allows a larger bandwidth to be processed at the cost of increased logic and multiplier resource utilization. In the case of the BEST-2 system two pipelined X-Engines, each processing 512 channels, are implemented in the firmware.

A two-stage accumulator is used to reduce the output data rate. The first stage is fixed to give a minimum integration time to 6.55 ms; this assures that the output bandwidth to each X-Engine is approximately equal to the input bandwidth. The second accumulator, implemented using QDR, is software controlled with integration lengths up to many minutes. A completed correlation matrix is sent to a receive computer over a 10 gigabit Ethernet (10 GbE) connection. Correlation matrices are packetized as User Datagram Protocol streams using the SPEAD protocol.[12]

2.3 S-Engine

In the BEST-2 backend described here, the requirements on the direct-imaging correlator are multifold. The system should be capable of generating images of the order of second time-scales, by the method described by Tegmark & Zaldarriaga (2009). Further, the system should be capable of passing formed beams at full bandwidth, i.e. without any accumulation, to downstream time-domain processing systems such as a real-time pulsar dedispersion engine (Magro et al. 2011).

Using a single frequency channel from each antenna element and the geometric array layout, a two-dimensional FFT is performed to produce an image. The two-dimensional *8-by-16* FFT is performed using an 8-point parallel input FFT followed by a corner-turn and 16-point parallel input FFT. Zero-padding is added to the signals from the 4×8 antenna BEST-2 array before input into each stage of the transform. This yields an output of 128 complex-valued beams, from which the power is calculated and accumulated. Each channel is cycled over to produce an image for each frequency band. The four-fold increase in the number of spatial transform outputs from

---

[11] https://casper.berkeley.edu/wiki/64ADCx64-12

[12] https://github.com/ska-sa/PySPEAD

zero-padding the inputs introduces a number of redundant calculations. The spatial transform produces 128 outputs but, as shown in Fig. 1(b), there are only 53 unique baselines in a 4×8 grid.

Accumulation takes place in two stages. A fixed 128-sample vector accumulator reduces the output of the FFT by summing 128 consecutive time samples of each beam for a single frequency channel. The complete set of 1024 channels and 128 beam powers can then be multiplexed into a single software-controllable vector accumulator in off-chip memory. Accumulations are packetized by the ROACH's PowerPC co-processor and sent to a data recorder over 1 GbE link using the same protocol as the FX correlator.

2.3.1 Beamformer

A total of 128 beams are generated with the spatial Fourier transform. Before calculating beam powers, eight arbitrary beams can be selected and output over 10 GbE at 16-bit precision for time-domain processing. Packets are constructed from multiple time and frequency samples from individual beams such that processing can be parellelized by beam across multiple machines. For a data word size W in bytes, a packet containing T samples and C channels has payload size $P = W \times T \times C$ bytes. In the BEST-2 backend, $W = 4$, and $T = 128$ is chosen to conveniently match the accumulation length of the imager. $C = 8$ is chosen to achieve packets with payloads of 4096 kB. These are generated with a simple data transpose in QDR memory space, and headers are inserted before transmission over 10 GbE. A pulsar and transient searching system for this output has been developed on graphics processing units by Magro, Hickish & Adami (2013).

Whilst the electric-field beams generated by spatial Fourier transform are suited to 'drift-scan' observations, software has been provided to switch beams to 'psuedo-track' up to eight simultaneous targets as they transit the primary beam. In this mode of operation, software will dynamically configure the S-Engine node outputs to transmit the nearest beam to a target source. This tracking method has the drawback that sources appearing between beam centres cannot be observed with the full sensitivity of the array. Fig. 2 shows the response of the seven synthesized beams covering a right-ascension range of 4°. Since neighbouring beams overlap at ∼81 per cent of peak power, signal-to-noise is reduced when tracking objects lie between pointing directions. Additionally, the beam centres vary with frequency. Since the fractional bandwidth of the BEST-2 analogue
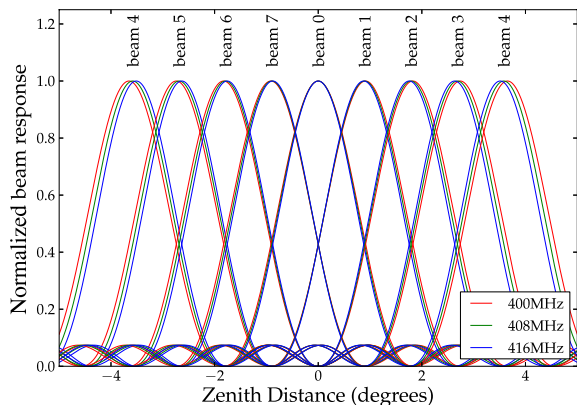

Figure 2. Theoretical beam responses (with aliases outside the primary beam removed) for an east–west strip of eight beams at 400, 408 and 416 MHz. Beam 4 is plotted twice, as its aliases give rise to equal beam response both east and west of the zenith.
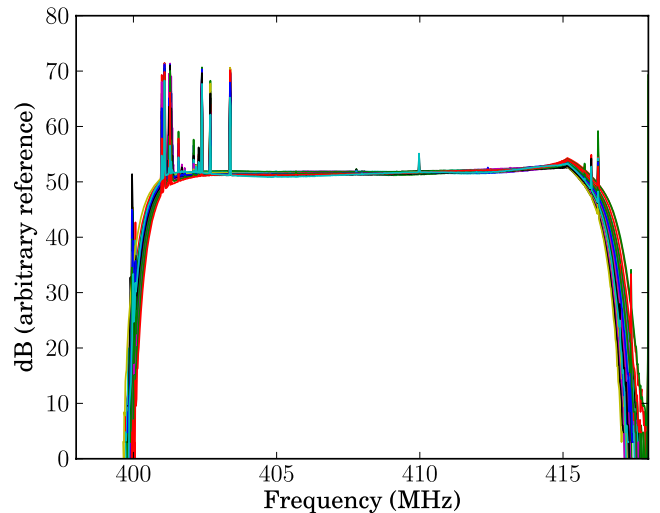

Figure 3. Autocorrelation spectra of 32 BEST-2 receivers after application of bandpass gain corrections.

front end is relatively small, this effect is limited, especially around the pointing centre of the telescope. The beams around the pointing centre are also preferred as they suffer least from spatial aliasing and primary beam gain attenuation.

3 INITIAL OBSERVATIONS

Instrumentation was installed and tested in 2012 March. Initial tests verified the F-Engine firmware during observations. Fig. 3 shows the autocorrelation spectra of the 32 receivers of the BEST-2 system after (Fig. 3) quantization equalization is applied to account for gain differences and band slope.

After installation, the FX correlator was used for observations of various bright radio sources. Since the Northern Cross is a transiting array, with primary beam pointing adjustable in declination, there is a limited period of time each day in which a source is in the primary beam. Bright sources, such as Cygnus A, Cassiopeia A and Taurus A, and a number of 3C sources were observed (Bennett 1962). Additionally, observations of multiple constant declination 24-h cycles were made.

In concurrency with the FX correlator observations, the direct-imaging correlator recorded data, initially in a 'raw' mode where no pre-calibration was applied and then in normal observational mode with complex gains solutions from the FX correlator applied in real time.

3.1 FX imaging

A transiting array provides a unique challenge of gain calibration since a source's apparent gain will change as it transits the primary beam. To account for this variation, a two-stage gain calibration method is used. Phase calibration and setting the flux scale are accomplished using Cassiopeia A and Cygnus A observations as point source sky models set to their Baars et al. (1977) flux levels and known spectral indices. Since these sources are very bright, only a few seconds at transit is needed produce a high signal-to-noise ratio data set to use for calibration. Over this period, the primary beam can be approximated as flat. A time-independent complex gain is derived for an initial calibration. After applying the gain corrections, an observation will be set to a flux scale relative to the flux of the calibration source. Each individual source is then
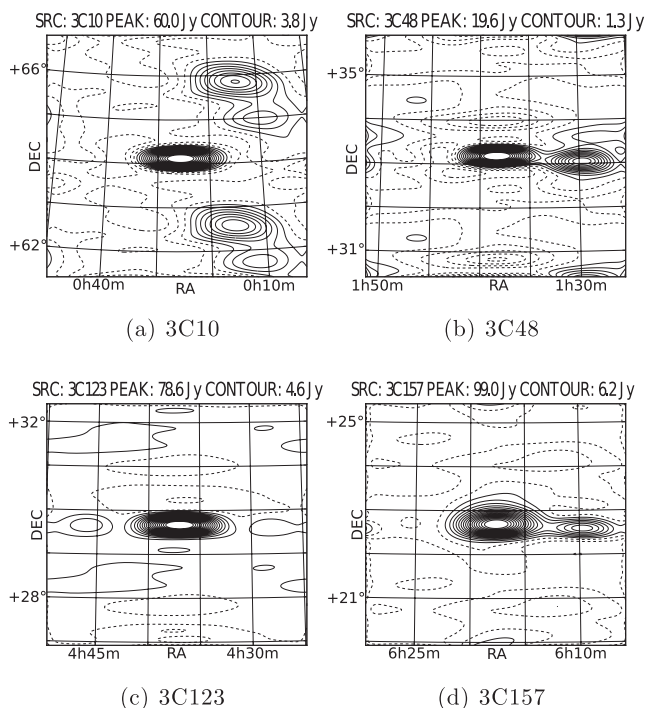
SRC: 3C10 PEAK: 60.0 Jy CONTOUR: 3.8 Jy

SRC: 3C48 PEAK: 19.6 Jy CONTOUR: 1.3 Jy

(a) 3C10

(b) 3C48

SRC: 3C123 PEAK: 78.6 Jy CONTOUR: 4.6 Jy

SRC: 3C157 PEAK: 99.0 Jy CONTOUR: 6.2 Jy

(c) 3C123

(d) 3C157

Figure 4. Calibrated 'snapshot' images of various 3C fields produced using the FX correlator; images have a noise level of ∼1.5 Jy.

calibrated in MeqTrees Noordam & Smirnov (2010) based on a local sky model taken from the 3C catalogue. A selection of images using this calibration method are shown in Fig. 4. An effect of the density of the antenna layout is a low field of view-to-PSF size ratio, ∼25 in the north–south direction and ∼7 in the east–west direction; thus, images tend to contain at most a few spatially separated point sources.

3.2 Direct imaging

The native output of the direct-imaging correlator is a 128 pixel image-domain data set where each pixel is a unique beam within the field of view. These 128 beams can be Fourier transformed to obtain samples in the uv domain. This produces summed visibilities corresponding to each of the 53 unique baselines, where each visibility is the average of all redundant baselines with a particular uv spacing. By transforming to the uv domain, we can compare the direct-imaging correlator data quality to that of our standard FX correlator.

3.2.1 Complex gain calibration

For our initial deployment, the FX correlator was used to derive complex gain solutions which were then applied to the direct-imaging correlator in real time during subsequent observations. Whilst the BEST-2 direct-imaging test-bed system utilizes the full correlator provided by the backend, it should be noted that an FX correlator which computes the full correlation matrix is not required for deriving gain calibrations. In order to make the direct-imaging architecture computationally beneficial, a smaller correlator, such as the calibration correlator included in LOFAR station firmware, or an offline correlator should be implemented.

In order to combine baseline data in a way that preserves signal-to-noise, a key requirement of the BEST-2 direct-imaging system is
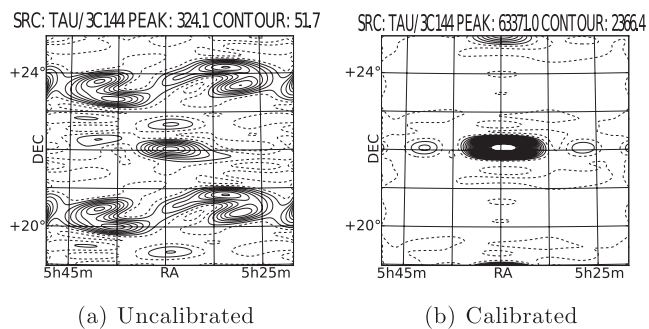

SRC: TAU/3C144 PEAK: 324.1 CONTOUR: 51.7

SRC: TAU/3C144 PEAK: 6337.0 CONTOUR: 2366.4

(a) Uncalibrated

(b) Calibrated

Figure 5. Dirty images of Taurus A produced from the direct-imager visibilities. Panel (a) shows the case before complex gain corrections are applied during observations and panel (b) shows that produced with complex gain corrections applied during observations.

the prior knowledge of gain corruptions in the receiving chains of each of the 32 receiving elements. Given the regular layout of antennas in this array, redundant-baseline calibration strategies such as those described by Noorishad et al. (2012) are applicable. However, we opt for a general sky-model-based algorithm which assumes prior knowledge of the sky observed by the telescope, but does not impose the condition that redundant baselines behave identically. This strategy is chosen for a number of reasons. The strong sidelobes of BEST-2 primary beams, which are not identical even amongst redundant baselines, make calibration challenging when there are bright sources away from the phase centre of the array. In such a situation, the assumption of redundant baselines breaks down and redundant-baseline calibration methods are likely to prove ineffective. Even without requiring baseline redundancy, varying sidelobe gains across the array makes for challenging calibration as gain corruptions are strongly direction dependent. To avoid this pitfall, the simplest calibration method is to wait for a transit of a bright source. In this case, the model sky is trivially a point source at the array phase centre from which gain solutions can be very easily extracted.

We use the column ratio gain estimation method, described by Boonstra & Veen (2001). Chosen for simplicity and ease of implementation, the algorithm uses ratios of antenna cross-correlations to estimate the diagonal (autocorrelation) elements of a measured visibility matrix in the absence of a system noise contribution. This allows creation of a modified correlation matrix and can subsequently be used, under the assumption of a model sky consisting of a point source at the phase centre, to obtain per-antenna gain solutions.

By applying gain solutions in the F-Engine during observations, there is a drastic change in image quality as seen in Fig. 5. An otherwise distorted image of the Taurus A field becomes a bright point source. The images in Fig. 5 have been obtained by first Fourier transforming the direct-imaging outputs into the uv domain where they, and the equivalent FX correlator outputs, are imaged using traditional synthesis imaging software.

During the imaging process, the choice of weighting schemes introduces a small technical hurdle for direct-imaging correlator visibilities. Since the effective baselines are an averaging of redundant baselines, using natural or uniform weighting in traditional imaging will produce equivalent results, that is a uniform weighted image, with direct-imaging correlator visibilities. In order to obtain the equivalent of a natural weighted FX correlator image, the visibilities obtained by the direct-imaging correlator are given weights
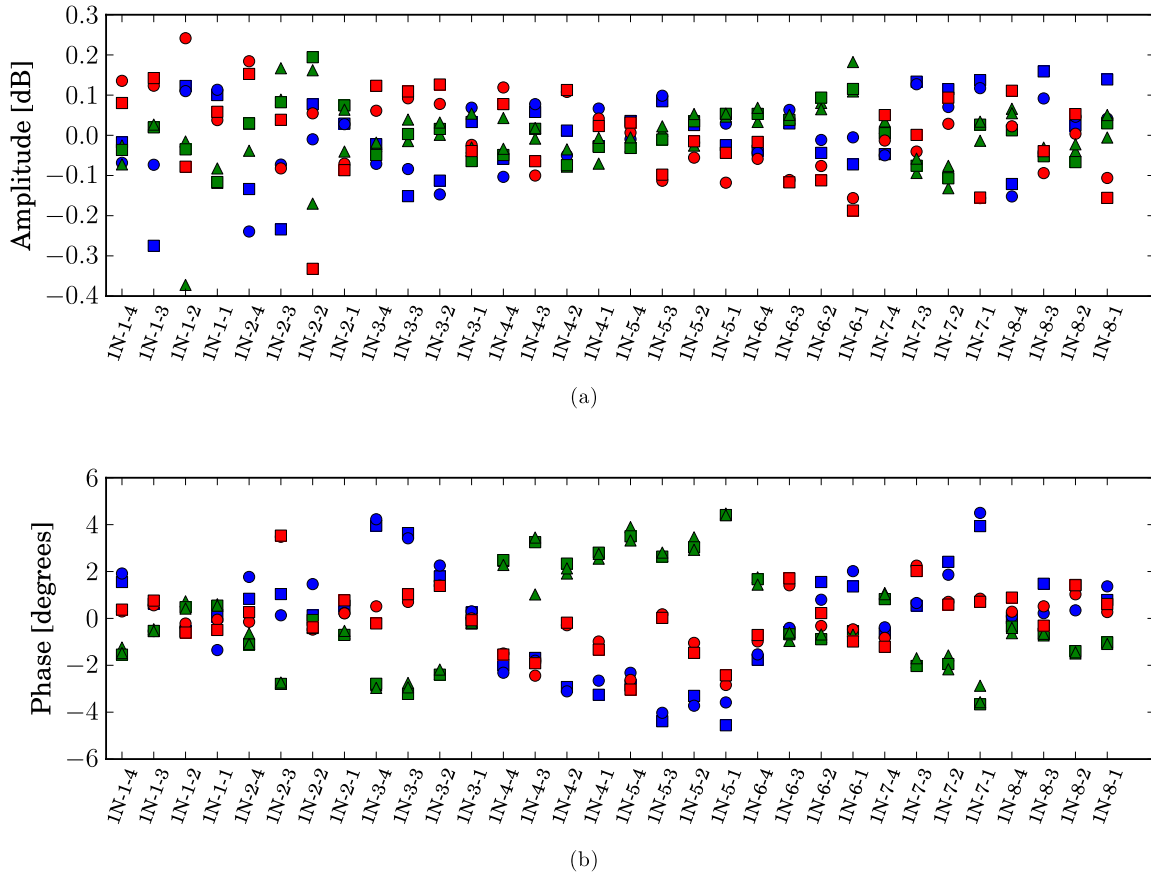
(a)

(b)

Figure 6. Complex gain solutions from seven calibration observations using Cassiopeia A (blue), Taurus A (green) and Cygnus A (red). The amplitude is stable to within less than a dB over the two-week period. The phase also remains stable, varying by only a few degrees in the same time period. There is an apparent solution bias based on the calibration source which is related to the array pointing angle.

based on their redundancies. In Fig. 5, we have used a natural weighted scheme.

3.2.2 System stability

Since we have implemented a calibration method which uses a single bright point source as our sky model, we need to consider the time-scale on which the gain solutions are accurate. Due to the transiting nature of BEST-2, we are limited to only a few calibration opportunities per day; thus, the calibration solutions need to be stable on at least multi-hour time-scales. Fig. 6 shows the amplitude and phase solutions from seven point source calibrations taken over a two-week period for each of the receiving elements. Over that period, the amplitude and phase remain stable. Calibration gains applied on day time-scales have proven sufficient during our initial observations.

3.3 Spatial FFT for beamforming

With the ability to calibrate antenna gains in real time in place, the unaccumulated outputs of the 2D FFT are calibrated electric-field beams on the sky. These beams remain fixed in position relative to the array location. Fig. 7 shows the apparent flux of Cassiopeia A as it transits across the array. Significant spatial aliasing effects are visible for all off-centre beams, becoming more severe for beams further from the array phase centre. This is a result of the hierarchical, analogue beamformer used in BEST-2, the first layer of which
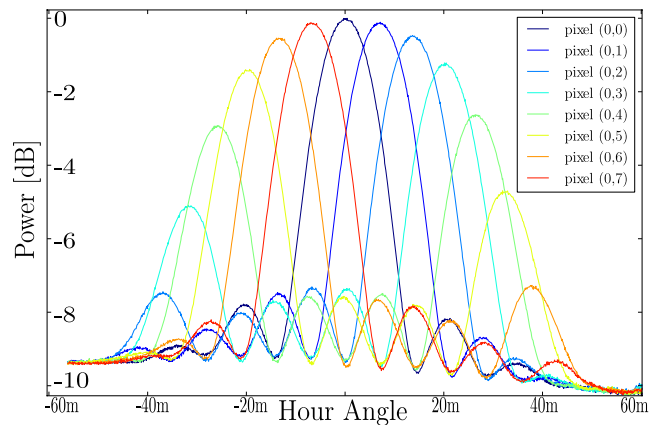

Figure 7. The normalized power observed in each of eight beams in an E-W array row during a transit of Cassiopeia A. The overall amplitude envelope is the primary beam response.

is the summation of 16 critically spaced dipoles. Fig. 7 also shows the loss of signal as the source moves between beams.

As noted earlier, this beamforming mode has already been put to use as the input to a pulsar and transient detection system (Magro et al. 2013). This system was verified by detection of pulsar B0329+54. After compensating for the DM of the pulsar, multiple pulses are summed to obtain a profile of the average pulse shape. Fig. 8 shows a profile of the average pulse shape with a profile from
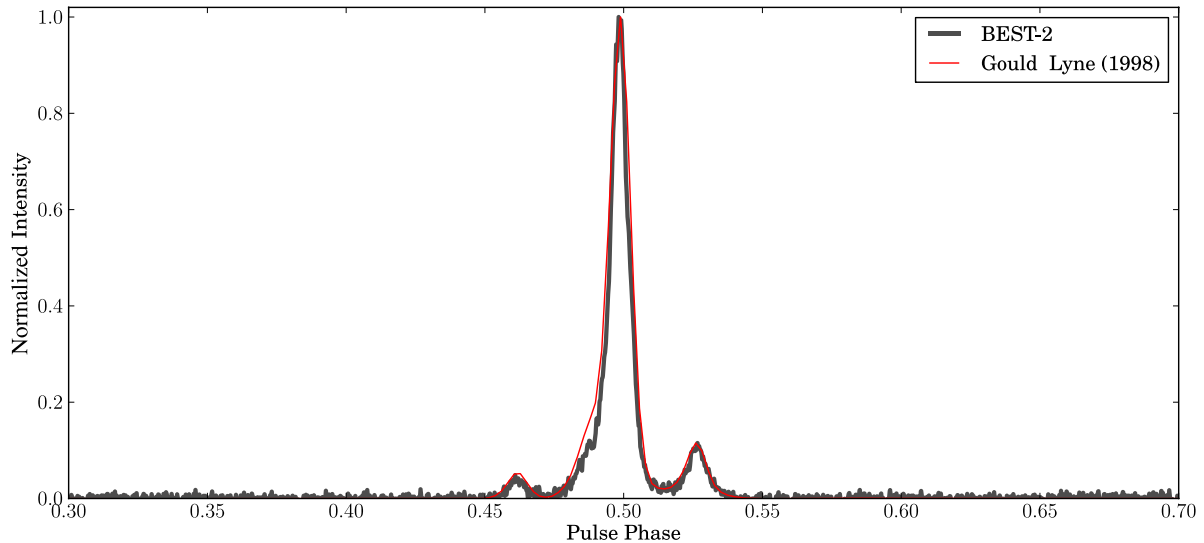
Figure 8. Folded profile (grey) of B0329+54 taken during an observation using BEST-2 with overplot (red) of 408 MHz Lovell Telescope archival data.

408 MHz Lovell Telescope archival data (Gould & Lyne 1998) overlaid. With access to a complete set of beams which cover the field of view, this system provides a promising platform for transient monitoring.

4 CONCLUSION

The main focus of this work has been on presenting a new digital backend for BEST-2 and showing the currently available features in the design. We have developed, deployed and tested an FPGA-based direct-imaging correlator and beamformer along with an concurrent FX correlator system for the BEST-2 array. Additionally, we have developed the necessary software for general use of this instrument; it is currently in regular use at the observatory. We have also touched on the data quality produced by the FX and direct-imaging correlators, and the beamformer. We have demonstrated detection of various astronomical sources with each of these instruments. In a supplementary work, we will present a study on the comparison of the FX and direct-imaging correlators. That work will focus on the usability of the direct imager for science observations, along with the challenge of calibrating such an instrument.

REFERENCES

Baars J. W. M., Genzel R., Pauliny-Toth I. I. K., Witzel A., 1977, A&A, 61, 99

Bennett A. S., 1962, Mem. R. Astron. Soc., 68, 163
Boonstra A. J., Veen A. J. V. D., 2001, Proc. 11th IEEE Statistical Signal Processing (SSP) Workshop, Gain Decomposition Methods for Radio Telescope Arrays. IEEE, New York, p. 365
Bunton J., 2011, IEEE Trans. Antennas Propag., 59, 2041
Gould D. M., Lyne A. G., 1998, MNRAS, 301, 235
Magro A., Karastergiou A., Salvini S., Mort B., Dulwich F., Zarb Adami K., 2011, MNRAS, 417, 2642
Magro A., Hickish J., Adami K. Z., 2013, J. Astron. Instrum., 2, 1350008
Montebugnoli S., Bartolini M., Bianchi G., Naldi G., Manley J., Parsons A., 2009a, in Torchinsky S. A., van Ardenne A., van den Brink-Havinga T., van Es A. J. J., Faulkner A. J., eds, Proc. Science, Wide Field Astronomy & Technology for the Square Kilometre Array (SKADS 2009), BEST Back End. SISSA, Trieste, p. 355
Montebugnoli S., Bianchi G., Monari J., Naldi G., Perini F., Schiaffino M., 2009b, in Torchinsky S. A., van Ardenne A., van den Brink-Havinga T., van Es A. J. J., Faulkner A. J., eds, Proc. Science, Wide Field Astronomy & Technology for the Square Kilometre Array (SKADS 2009), BEST: Basic Element for SKA Training. SISSA, Trieste, p. 331
Morales M. F., 2011, PASP, 123, 1265
Noordam J. E., Smirnov O. M., 2010, A&A, 524, A61
Noorishad P., Wijnholds S. J., van Ardenne A., van der Hulst T., 2012, A&A, 16
Otobe E. et al., 1994, PASJ, 46, 503
Parsons A. et al., 2006, Fortieth Asilomar Conference on Signals, Systems and Computers, PetaOp/Second FPGA Signal Processing for SETI and Radio Astronomy. Pacific Grove, California, p. 2031
Parsons A., Pober J., McQuinn M., Jacobs D., Aguirre J., 2012, AJ, 753, 81
Perini F., 2009, in Torchinsky S. A., van Ardenne A., van den Brink-Havinga T., van Es A. J. J., Faulkner A. J., eds, Proc. Science, Wide Field Astronomy & Technology for the Square Kilometre Array (SKADS 2009), Low Noise Design Experience for the SKADS/BEST Demonstrator. SISSA, Trieste, p. 341
Perini F., Bianchi G., Schiaffino M., Monari J., 2009, in Torchinsky S. A., van Ardenne A., van den Brink-Havinga T., van Es A. J. J., Faulkner A. J., eds, Proc. Science, Wide Field Astronomy & Technology for the Square Kilometre Array (SKADS 2009), BEST Receiver Experience: General Architecture, Design and Integration. SISSA, Trieste, p. 351
Romney J. D., 1999, in Taylor G. B., Carilli C. L., Perley R. A., eds, ASP Conf. Ser. Vol. 180, Synthesis Imaging in Radio Astronomy II. Astron. Soc. Pac., San Francisco, p. 57
Tegmark M., Zaldarriaga M., 2009, Phys. Rev. D, 79, 083530

Tegmark M., Zaldarriaga M., 2010, Phys. Rev. D, 82, 103501

Thompson A. R., Moran J. M., Swenson G. W., Jr, 2004, Interferometry and Synthesis in Radio Astronomy, 2nd edn. Wiley-VCH, Berlin

Urry W., Wright M., Dexter M., MacMahon D., 2007, Technical report 73, ATA Memo: The ATA Correlator. Univ. California, Berkeley

Williams J. R., 1968, J. Acoust. Soc. Am., 44, 1454

Zheng H. et al., 2013, IEEE International Symposium on Phased Array Systems & Technology, Mapping Our Universe in 3D with MITEoR, p. 784

SUPPORTING INFORMATION

Additional Supporting Information may be found in the online version of this article:

Appendix. Instrumentation block diagrams. (http://mnras.oxfordjournals.org/ lookup/suppl/doi:10.1093/mnras/ stu188/-/DC1)

Please note: Oxford University Press is not responsible for the content or functionality of any supporting materials supplied by the authors. Any queries (other than missing material) should be directed to the corresponding author for the article.

This paper has been typeset from a TEX/LATEX file prepared by the author.